

Supersolid-like square- and triangular-lattice crystallization of dipolar droplets in a box trap

Luis E. Young-S.* · S. K. Adhikari**

Received: date / Accepted: date

Abstract Using a beyond-mean-field model including a Lee-Huang-Yang-type interaction, we demonstrate a supersolid-like spatially-periodic square- and triangular-lattice crystallization of droplets in a polarized dipolar condensate confined by an appropriate three-dimensional (3D) box trap. In this paper we consider a rectangular box (cuboid) trap, a square box (cuboid with two equal sides) trap, a cylindrical box trap and a hexagonal box (hexagonal prism) trap. The droplet lattice is always formed in the x - y plane perpendicular to the polarization z direction of dipolar atoms. In contrast to a harmonic trap, the box traps allow the formation of a large clean supersolid-like spatially-periodic crystallization in free space without any distortion. Moreover, a droplet lattice can be formed in a 3D box trap with a significantly reduced number of atoms than in a harmonic trap, which could facilitate the experimental observation of droplet lattice in a box trap. With present know-how such a supersolid-like crystallization of dipolar droplets in a 3D box trap can be realized in a laboratory thus allowing the study of a large periodic lattice of dipolar droplets in free space bounded by rigid walls.

Keywords Bose-Einstein condensate · dipolar atoms · supersolid · square lattice · triangular lattice

1 Introduction

A supersolid [1–6] is a special quantum state of matter with a rigid spatially-periodic crystalline structure [7], breaking continuous translational invariance, that flows with zero viscosity as a superfluid breaking continuous gauge invariance.

Hence, a supersolid simultaneously possesses the properties of a crystalline solid and a superfluid in contradiction with the belief that a frictionless flow is a property exclusive to a superfluid. The initial search of supersolidity in solid ^4He [8] was not successful [9]. However, there had been theoretical suggestions for creating a supersolid in a spin-orbit (SO) coupled spinor Bose-Einstein condensate (BEC) [10–12], in a dipolar BEC [13, 14], and in a BEC with finite-range atomic interaction [15]. After the recent experimental observation of supersolids in a quasi-one-dimensional (quasi-1D) SO-coupled pseudo spin-1/2 spinor BEC [16] and in a quasi-1D [17–19] polarized dipolar BEC, the study of supersolids has drawn a great deal of attention among research workers in low-temperature and condensed matter physics. Specifically, for an appropriate number of atoms N and for an appropriate mixture of contact and dipolar interactions, high-density droplet-formation was observed experimentally in a strongly dipolar harmonically-trapped BEC of ^{164}Dy [20] and ^{168}Er [21] atoms. For a strongly dipolar BEC and for a sufficiently large number of atoms N , as the density of atoms reaches a critical value, due to the strong dipolar attraction, the trapped dipolar BEC shrinks to a very small size and a tiny droplet of size much smaller than the harmonical oscillator trap lengths, is formed as first observed [22] in a quasi-two-dimensional (quasi-2D) dipolar BEC of ^{164}Dy atoms. However, such a droplet can accommodate a maximum number of atoms. With further increase of N , multiple droplets arranged along a straight line [17–19, 23, 24], for a quasi-1D configuration, or on a spatially-periodic triangular [22, 25] or square [26] lattice, in a quasi-2D configuration, can be formed.

In the framework of a mean-field Gross-Pitaevskii (GP) equation, a sufficiently strongly dipolar BEC, for a large number of atoms or for a large atomic dipole moment, collapses. Nevertheless, a beyond-mean-field Lee-Huang-Yang-type [27] (LHY-type) repulsive interaction [28, 29], with

*Grupo de Modelado Computacional, Facultad de Ciencias Exactas y Naturales, Universidad de Cartagena, 130014 Cartagena, Bolívar, Colombia · **Instituto de Física Teórica, UNESP - Universidade Estadual Paulista, 01.140-070 São Paulo, São Paulo, Brazil

a higher-order quartic repulsive nonlinearity, compared to the cubic nonlinearity of the GP equation, can stop the collapse and form a stable droplet in a harmonically-trapped strongly dipolar BEC [14, 30, 31]. This beyond-mean-field model with the LHY-type interaction [28, 29] has been successfully used in the study of droplets and droplet lattice in a harmonically-trapped dipolar BEC in both quasi-1D [17–19, 23, 24] and quasi-2D [22, 25, 32, 33] configurations.

In a quasi-1D harmonically-trapped dipolar BEC of polarized ^{164}Dy [19, 23, 24], ^{162}Dy [17, 18, 34], and ^{166}Er [19, 24] atoms, a spontaneous spatially-periodic crystallization of droplets in a straight line was observed, whereas in a quasi-2D harmonically-trapped dipolar BEC of polarized ^{164}Dy atoms [22, 25], a spatially-periodic crystallization of droplets on a triangular lattice was observed. These linear [35, 36] and triangular-lattice [33, 37–40] crystallization of droplets were also confirmed in theoretical studies using three-dimensional (3D) beyond-mean-field models with the LHY-type interaction. More recently, the formation of a spatially-periodic square-lattice pattern of droplets in a harmonically-trapped dipolar BEC was demonstrated [26] in a theoretical study using a beyond-mean-field model. Nevertheless, in most of these investigations, specially in the numerical studies on a truncated finite system as in this paper, the relation of these quasi-1D and quasi-2D spatially-periodic states to supersolidity was not established [41]. That task requires a demonstration of the spontaneous breakdown of gauge symmetry (giving the superfluid order parameter) and the spontaneous breakdown of translational symmetry in these systems. Lacking such a rigorous demonstration of supersolidity, in this paper we call these spatially-periodic states supersolid-like states as in some previous studies on quasi-2D SO-coupled spinor BECs [42, 43].

In this paper, we demonstrate and study numerically by imaginary-time propagation a spatially-periodic quasi-2D crystallization of dipolar droplets on triangular and square lattices through the formation of droplet-lattice states in the x - y plane, perpendicular to the polarization z direction of dipolar atoms, in a 3D box trap, using a beyond-mean-field model including the LHY-type interaction. The dynamical stability of these droplet-lattice states was established by real-time propagation over a long period of time after introducing a perturbation at time $t = 0$. One has a uniform potential inside a box trap and an infinite potential outside, such that the wave function is zero on the boundary of the box. Thus a 3D box trap allows the formation and study of droplets in free space with a uniform potential bounded by a rigid wall, without an interfering harmonic oscillator potential, as in other studies, thus resulting in a few advantages. We find that an increase in the size of the box trap allows the formation of a very large lattice of droplets in a uniform potential with a significantly smaller number of atoms per droplet without any visible distortion, and with a much reduced uniform

background atom cloud, when compared to the previous results [26, 33] obtained with a harmonic trap, which could be an advantage for the experimental study of a spatially-periodic quasi-2D crystallization of dipolar droplets in a box trap.

Recently, BECs were created experimentally in a quasi-1D [44–46], and 3D [47–51] box traps. The quasi-1D [44–46] trap has uniform confinement along one direction and harmonic confinement in transverse directions. The 3D optical trap of Refs. [47–51] is a uniform 3D cylindrical box trap which has a circular box trap in x - y plane with a uniform confinement in z direction. The experimental technique now allows the creation of a combination of box trap and harmonic trap in x , y and z directions. In the x - y plane one can create a circular box trap or a square box trap coupled to a box trap along the z direction. Box traps are now regularly used in experimental and theoretical studies of cold atoms [52–56]. In this paper we will consider the following traps: a 3D square box (a cuboid with two equal sides) trap U_A , a 3D rectangular box (a cuboid) trap U_B , a cylindrical box trap U_C , and a hexagonal box (hexagonal prism) trap U_D . We demonstrate the formation of a square-lattice crystallization of droplets in traps U_A , U_B and U_C and a triangular-lattice crystallization of droplets in traps U_B , U_C and U_D . We find that the symmetry of the final state in numerical simulation is sensitive to the initial state employed. A final state with a specific symmetry — a square, or a triangular lattice — can easily be obtained with the use of an initial state with the same symmetry. No such supersolid-like state can be obtained in a trapped BEC with isotropic contact interaction. In a dipolar BEC, a single droplet is stable for the number of atoms below a critical value N_{crit} . As the number of atoms increases beyond N_{crit} , a single-droplet state becomes energetically unstable and collapses and stable multiple droplets are created and due to an interplay between the binding box potential and dipolar repulsion in the x – y plane, a supersolid-like arrangement of droplets is formed.

In Sec. 2 the beyond-mean-field model with the LHY-type interaction is presented. In Sec. 3 we present the numerical results for stationary states with two types of periodic array of droplets, e.g. square and triangular lattice, in a dipolar BEC confined by an appropriate box trap. A square-lattice arrangement of droplets is possible in a square box trap U_A , U_B and U_C . For the formation of a triangular-lattice arrangement of droplets we considered an appropriate rectangular box trap U_B , a cylindrical box trap U_C , and a hexagonal box trap U_D . The square box trap U_A is the most appropriate for generating a square lattice of dipolar droplets and the hexagonal box trap U_D is the most suitable for generating a triangular lattice of droplets. Finally, in Sec. 4 we present a summary of our findings.

2 Beyond-Mean-field model

In this study we consider a 3D beyond-mean-field model including an appropriate LHY-type interaction [28, 29]. We consider a BEC of N dipolar atoms, of mass m each, polarized along the z direction, interacting through the following atomic contact and dipolar interactions [57–59]

$$V(\mathbf{R}) = \frac{4\pi\hbar^2 a}{m} \delta(\mathbf{R}) + \frac{\mu_0 \mu^2}{4\pi} \frac{1 - 3\cos^2 \theta}{|\mathbf{R}|^3}, \quad (1)$$

where μ_0 is the permeability of vacuum, a is the scattering length, μ is the magnetic moment of each atom, $\mathbf{R} = \mathbf{r} - \mathbf{r}'$ is the vector joining two atoms placed at $\mathbf{r} \equiv \{\mathbf{x}, \mathbf{y}, \mathbf{z}\}$ and $\mathbf{r}' \equiv \{\mathbf{x}', \mathbf{y}', \mathbf{z}'\}$ with θ the angle between vector \mathbf{R} and the z axis. It is convenient to introduce the following dipolar length to quantify the strength of dipolar interaction

$$a_{\text{dd}} = \frac{\mu_0 \mu^2 m}{12\pi\hbar^2}. \quad (2)$$

The dimensionless ratio

$$\epsilon_{\text{dd}} \equiv \frac{a_{\text{dd}}}{a} \quad (3)$$

defines the relative strength of dipolar and contact interactions.

A dipolar BEC is described by the following 3D beyond-mean-field equation with the LHY-type interaction [31, 33, 57–59]

$$i\hbar \frac{\partial \psi(\mathbf{r}, t)}{\partial t} = \frac{\hbar^2}{m} \left[-\frac{1}{2} \nabla^2 + \frac{m}{\hbar^2} U(\mathbf{r}) + 4\pi a N |\psi(\mathbf{r}, t)|^2 \right. \\ \left. + 3a_{\text{dd}} N \int \frac{1 - 3\cos^2 \theta}{|\mathbf{R}|^3} |\psi(\mathbf{r}', t)|^2 d\mathbf{r}' \right. \\ \left. + \gamma_{\text{QF}} |\psi(\mathbf{r}, t)|^3 \right] \psi(\mathbf{r}, t), \quad (4)$$

where $i = \sqrt{-1}$, $U(\mathbf{r})$ is the box trap and the wave-function normalization is $\int |\psi(\mathbf{r}, t)|^2 d\mathbf{r} = 1$. The third and the fourth terms on the right-hand-side of Eq. (4) are contributions of atomic contact and dipolar interactions and the last term is the contribution of the beyond-mean-field LHY-type interaction with the coefficient γ_{QF} given by [28, 29, 31]

$$\gamma_{\text{QF}} = \frac{128}{3} \sqrt{\pi a^5} Q_5(\epsilon_{\text{dd}}), \quad (5)$$

where the function

$$Q_5(\epsilon_{\text{dd}}) = \int_0^1 dx (1 - x + 3x\epsilon_{\text{dd}})^{5/2} \quad (6)$$

can be evaluated to yield the following expression for the coefficient γ_{QF} [31]

$$\gamma_{\text{QF}} = \frac{128}{3} \sqrt{\pi a^5} \frac{(3\epsilon_{\text{dd}})^{5/2}}{48} \left[(8 + 26\epsilon + 33\epsilon^2) \sqrt{1 + \epsilon} \right. \\ \left. + 15\epsilon^3 \ln \left(\frac{1 + \sqrt{1 + \epsilon}}{\sqrt{\epsilon}} \right) \right], \quad \epsilon = \frac{1 - \epsilon_{\text{dd}}}{3\epsilon_{\text{dd}}}. \quad (7)$$

Actually, the function $Q_5(\epsilon_{\text{dd}})$, as well as the coefficient γ_{QF} , representing a beyond-mean-field LHY-type correction

for dipolar atoms, is complex for $\epsilon_{\text{dd}} > 1$ and, for studies of stationary states, expression (7) is formally meaningful only for $\epsilon_{\text{dd}} \leq 1$, where this expression is real [60]. However its imaginary part remains small compared to its real part for medium values of a used in this paper $a \approx 85a_0$ and will be neglected in this study of stationary self-bound states as in other studies.

Equation (4) can be reduced to the following dimensionless form by scaling lengths in units of a length scale l , time in unit of ml^2/\hbar , energy in unit of \hbar^2/ml^2 , and density $|\psi|^2$ in unit of l^{-3}

$$i \frac{\partial \psi(\mathbf{r}, t)}{\partial t} = \left[-\frac{1}{2} \nabla^2 + U(\mathbf{r}) + 4\pi a N |\psi(\mathbf{r}, t)|^2 \right. \\ \left. + 3a_{\text{dd}} N \int \frac{1 - 3\cos^2 \theta}{|\mathbf{R}|^3} |\psi(\mathbf{r}', t)|^2 d\mathbf{r}' \right. \\ \left. + \gamma_{\text{QF}} N^{3/2} |\psi(\mathbf{r}, t)|^3 \right] \psi(\mathbf{r}, t), \quad (8)$$

where we are using the same functions to represent the scaled (and original unscaled) variables.

In this study we will consider the following box traps: (U_A) a square box (a cuboid with two equal sides) trap defined by $U(\mathbf{r}) = 0$ for $|x| < l_1$, $|y| < l_2 = l_1$ and $|z| < l_3$ and infinite otherwise, where l_1, l_2, l_3 are the lengths of the orthogonal box trap; (U_B) a rectangular box (a cuboid) trap defined by $U(\mathbf{r}) = 0$ for $|x| < l_1$, $|y| < l_2$ and $|z| < l_3$ and infinite otherwise; (U_C) a 3D cylindrical box trap, now routinely used in experiments [47–49], defined by $U(\mathbf{r}) = 0$ for $\rho \equiv \sqrt{x^2 + y^2} < l_1$ and $|z| < l_3$ and infinite otherwise, where l_1 is the radius of the cylindrical box trap and l_3 is its length; (U_D) a 3D hexagonal (hexagonal prism) box trap defined by $U(\mathbf{r}) = 0$ for $|x| < \sqrt{3}l_1/2$, $|\pm x + \sqrt{3}y| < \sqrt{3}l_1$ and $|z| < l_3$ and infinite otherwise, where l_1 is the length of each side of the hexagonal box and l_3 is its length.

3 Numerical Results

The partial differential equation (8) for a dipolar BEC is solved numerically employing the split-time-step Crank-Nicolson method [61] by time propagation, using C or FORTRAN programs [58] or their open-multiprocessing versions [62]. We used imaginary-time propagation for a stationary state and real-time propagation for studying dynamics [61, 63]. Often, the density of the system has large extension in the x - y plane and it is appropriate to take a smaller number of discretization steps along z direction as compared to the same along x and y directions. We take space step $\Delta = 0.05$ in all three directions – x, y , and z – and a time step $0.1\Delta^2$ in imaginary-time propagation and a time step $0.05\Delta^2$ in real-time propagation and verified that the presented numerical results converged with respect to a reduction of space and time steps. Due to the divergent $1/|\mathbf{R}|^3$ term, it is problematic to treat the nonlocal dipolar interaction integral numerically in the beyond-mean-free model (8) in configuration

space. To avoid this problem, the dipolar term is calculated in the momentum space by a Fourier transformation using a convolution identity [58], which is economic numerically due to the smooth behavior of this term in momentum space. The Fourier transformation of the dipolar potential has an analytic result [58] which enhances the accuracy of the numerical procedure. After obtaining the solution in momentum space, the result in configuration space is obtained by an inverse Fourier transformation.

We present results for a BEC of strongly dipolar ^{164}Dy atom, as many of the experimental [20, 22, 25] and related theoretical [33, 37–40] studies were performed with this atom. In this study we will take the scaling length $l = 1 \mu\text{m}$ as the unit of length, so that the unit of density $|\psi|^2$ is $1 \mu\text{m}^{-3}$ and evaluate the results in dimensionless units. For the formation of a square- or a triangular-lattice of droplets we need a strongly dipolar atom with $\epsilon_{\text{dd}} > 1$ [22], while the dipolar interaction dominates over the contact interaction. The experimental estimate of scattering length of ^{164}Dy atom is $a = (92 \pm 8)a_0$ [64] and its dipolar length is $a_{\text{dd}} = 130.8a_0$ corresponding to the magnetic dipole moment $10\mu_B$, where a_0 is the Bohr radius and μ_B is the Bohr magneton. In this study we take $a = 85a_0$, as in a previous study of droplets [26]; consequently, $\epsilon_{\text{dd}} = 1.5388... > 1$. This value of scattering length was used in a previous study of droplet lattice in presence of harmonic trapping potentials [26] and is close to its experimental estimate and also to the values $a = 88a_0$ [25, 32, 33] and $a = 70a_0$ [37] used in other studies of formation of quantum droplets in a quasi-2D harmonically trapped dipolar BEC.

An appropriate choice of the initial state is essential for an efficient evaluation of a droplet-lattice arrangement employing imaginary-time propagation [26]. The numerical simulation of a few-droplet state can be performed by employing a Gaussian initial function, viz. Fig. 1. The numerical evaluation of a large square- or a triangular-lattice crystallization was started by an initial analytic wave function with a lattice structure of appropriately placed Gaussian droplets on a square or a triangular lattice, respectively [26]. For example, the numerical simulation of a 81-droplet 9×9 square-lattice state was initiated by the following analytic initial wave function with 81 Gaussian droplets appropriately placed on a square lattice:

$$\phi(\mathbf{r}) \sim \sum_{i,j=0}^{\pm 1, \pm 2, \pm 3, \pm 4} e^{-(x+i\beta)^2 - (y+j\beta)^2} e^{-z^2/\alpha^2} \quad (9)$$

with the lattice constant $\beta \approx 5$ and an appropriately chosen z -width α . Similarly, the numerical simulation of a 37-droplet triangular-lattice state is initiated by the following analytic initial function with 37 droplets appropriately placed on a triangular lattice:

$$\phi(\mathbf{r}) \sim \left[\sum_{i=0}^{\pm 1, \pm 2, \pm 3} e^{-(x+4i\beta)^2 - y^2} \right]$$

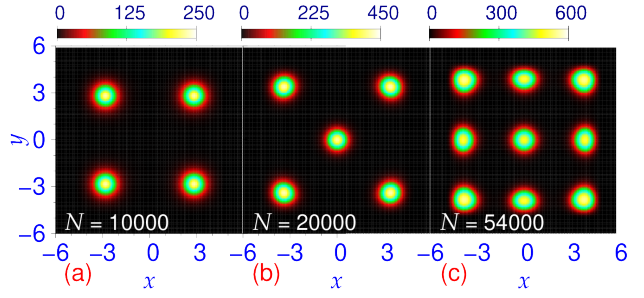


Fig. 1 Contour plot of density of ^{164}Dy atoms $N|\psi(x,y,0)|^2$ in the x - y plane in (a) square-lattice crystallization of 4 droplets, (b) centered square-lattice crystallization of 5 droplets, and (c) square-lattice crystallization of 9 droplets, in a 3D cube box trap U_A . The initial state used in the evaluation of these states was a *single Gaussian* state which evolves to multiple-droplet final states. The x , y and z lengths of the box potential are $l_1 = l_2 = l_3 = 5$ and $a = 85a_0$. Plotted quantities in all figures are dimensionless and the corresponding number of atoms N is displayed in all plots of this paper. The actual 3D density can be obtained using the length scale $l = 0.607 \mu\text{m}$; for example, the maximum density in (c) is $604/l^3 \approx 2.8 \times 10^{21} \text{ m}^{-3}$.

$$\begin{aligned} & + \sum_{i=\pm 1, \pm 3, \pm 5} \sum_{j=\pm 1} e^{-(x+2i\beta)^2 - (y+2\sqrt{3}j\beta)^2} \\ & + \sum_{i=0, \pm 2, \pm 4} \sum_{j=\pm 2} e^{-(x+2i\beta)^2 - (y+2\sqrt{3}j\beta)^2} \\ & + \sum_{i=\pm 1, \pm 3} \sum_{j=\pm 3} e^{-(x+2i\beta)^2 - (y+2\sqrt{3}j\beta)^2} \Big] e^{-z^2/\alpha^2}. \quad (10) \end{aligned}$$

The initial analytic functions in other cases are chosen appropriately.

For a harmonically-trapped specific dipolar BEC with a given a and a_{dd} there is a typical lattice constant (length). For a dipolar BEC of ^{164}Dy atoms with $a = 85a_0$ this lattice constant is approximately $\sim 4 \mu\text{m}$ in the trap of Ref. [26]. As the number of atoms in that harmonically-trapped ^{164}Dy BEC is increased, more and more droplets are formed and a larger lattice is generated filling a larger space maintaining approximately the same lattice spacing. This lattice spacing for a dipolar BEC of ^{164}Dy atoms is approximately the same for a box trap. A square-lattice state is efficiently generated in a square or a rectangular box trap, whereas a triangular-lattice state is efficiently generated in a hexagonal box trap. Because of the rigid walls of the box trap and because of large long-range dipolar repulsion the droplets near the boundary will be arranged with the same symmetry as the box potential which will influence the droplets further in the bulk to follow the same symmetry and eventually fill in the whole inner space. To generate a specific droplet-lattice state one should consider a box trap which could accommodate the same. For example, as the lattice constant is approximately ~ 4 in the box trap, the extension of a 25-droplet 5×5 square-lattice state in the x - y plane is about 20×20 . Hence, the x and y lengths of a square box trap U_A should be about $l_1 = l_2 \approx 10$. For a 49-droplet square-lattice

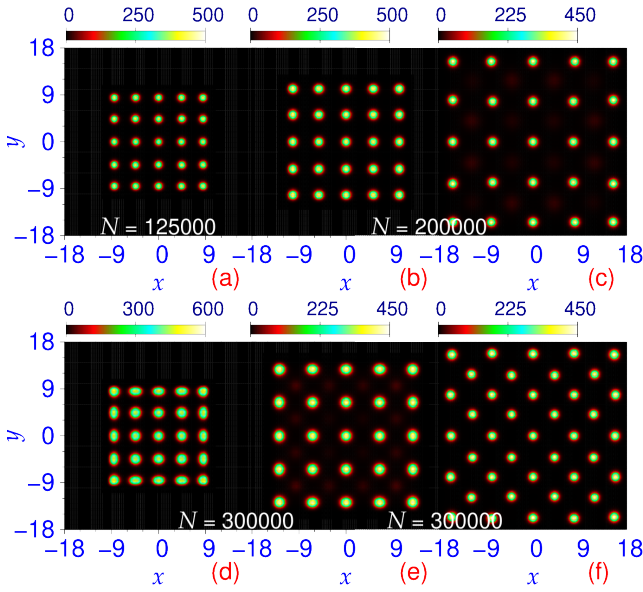


Fig. 2 Contour plot of density of ^{164}Dy atoms $N|\psi(x,y,0)|^2$ in the x - y plane of square-lattice crystallization of 25 droplets for (a) $N = 125000$, with x and y lengths $l_1 = l_2 = 10$, (b) $N = 200000$, with $l_1 = l_2 = 12$, (c) $N = 200000$, with $l_1 = l_2 = 18$, (d) $N = 300000$, with $l_1 = l_2 = 10$, (e) $N = 300000$, with $l_1 = l_2 = 15$, (f) $N = 300000$, with $l_1 = l_2 = 18$, in a 3D square box trap U_A . The z -length in all cases is $l_3 = 5$ and $a = 85a_0$. The initial state in these imaginary-time simulations [including the state in (f)] is an analytic 25-droplet 5×5 state arranged on a square lattice, viz. Eq. (9).

state the x and y lengths should be slightly larger and about $l_1 = l_2 \approx 15$. The extension of a droplet in the z direction is about a few length units and in all calculations we will take the length of the box trap to be $l_3 = 5$. In addition one should have an appropriate number of atoms in the BEC to form a certain number of droplets, as a minimum number of atoms is needed to form a new droplets.

First we consider the spontaneous formation of droplets on a square lattice in the box trap U_A . For this purpose we consider a cubic box trap, which is a special case of a square box trap with equal x , y and z -lengths: $l_1 = l_2 = l_3 = 5$. In numerical simulation by imaginary-time propagation, we consider an analytic Gaussian initial state with a small number of atoms ($N < 5000$). The final state is also found to be an extended state occupying almost the whole box (result not shown here). As the number of atoms is increased approximately to $N \approx 10000$, four droplets arranged on a square lattice are formed spontaneously from an analytic initial Gaussian state in imaginary-time calculation. This is illustrated through a contour plot of density of ^{164}Dy atoms $N|\psi(x,y,0)|^2$ in the x - y plane in Fig. 1(a) for $N = 10000$. We could not find a one-, two-, or three-droplet state in this cubic box trap U_A for smaller N ($N < 10000$). As the number of atoms is increased further to $N \approx 20000$, five droplets arranged on a centered square lattice are formed as shown in Fig. 1(b) through a contour plot of density of ^{164}Dy atoms

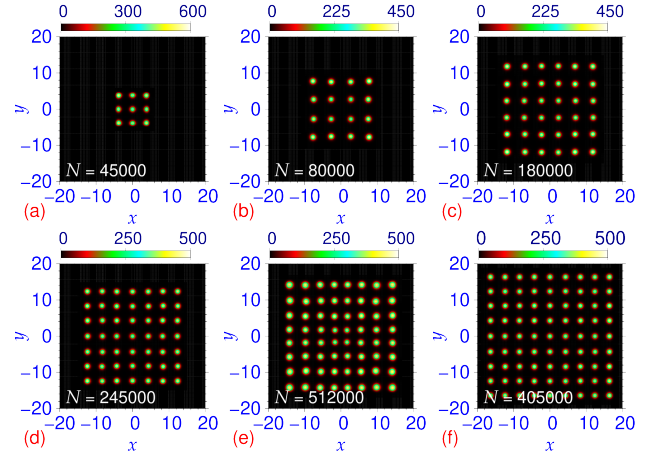


Fig. 3 Contour plot of density of ^{164}Dy atoms $N|\psi(x,y,0)|^2$ in the x - y plane of square-lattice crystallization of (a) 9 droplets with x and y lengths $l_1 = l_2 = 5$, (b) 16 droplets with $l_1 = l_2 = 10$, (c) 36 droplets with $l_1 = l_2 = 15$, (d) 49 droplets with $l_1 = l_2 = 15$, (e) 64 droplets with $l_1 = l_2 = 16$, (f) 81 droplets with $l_1 = l_2 = 18$, in a 3D square box trap U_A . The z -length in all cases is $l_3 = 5$ and $a = 85a_0$.

$N|\psi(x,y,0)|^2$ in the x - y plane for $N = 20000$ atoms. The five-droplet state continue to exist as the unique possible droplet state for N up to ≈ 50000 , although the size of the droplet becomes larger as the number of atoms is increased. For larger values of N ($N > 50000$), for this cubic box trap, a nine-droplet state appears in imaginary-time simulation from an analytic Gaussian initial state as illustrated in Fig. 1(c) through a contour plot of density $N|\psi(x,y,0)|^2$ of ^{164}Dy atoms $N|\psi(x,y,0)|^2$ in the x - y plane for $N = 54000$ atoms. We could not find a six-, seven-, or eight-droplet state in this cubic box trap U_A for any N , indicating that the system prefers these spatially-periodic ordered square-lattice states in a square box trap. We will see that these two arrangements – square lattice in (a) and (c) and centered square lattice in (b) – are the most likely unit cells for large droplet-lattice formation in a square box trap as the size of the square box trap and number of atoms are increased so as to form and accommodate a large number of droplets on a square lattice for a large number of atoms in a larger space. A distorted lattice state will be generated unless the size of the box trap is increased as the number of atoms is increased.

To demonstrate the formation of a specific droplet-lattice state for different number of atoms in the square box trap U_A , we consider a 25-droplet square-lattice state for different number of atoms and different sizes (lengths $l_1 = l_2$) of a square box trap U_A . In Fig. 2 we display the contour plot of density of ^{164}Dy atoms $N|\psi(x,y,0)|^2$ in the x - y plane for (a) $N = 125000$, $l_1 = l_2 = 10$, (b) $N = 200000$, $l_1 = l_2 = 12$, (c) $N = 200000$, $l_1 = l_2 = 18$, (d) $N = 300000$, $l_1 = l_2 = 10$, (e) $N = 300000$, $l_1 = l_2 = 15$, (f) $N = 300000$, $l_1 = l_2 = 18$. In all cases the z -length is $l_3 = 5$ and the initial state in imaginary-time propagation was an analytic 25-droplet state

arranged on a 5×5 square lattice, viz. Eq. (9). In the first five cases displayed in (a)-(e), the final state is also a 25-droplet state arranged on a 5×5 square lattice, although the size of the droplet lattice (and also that of the unit cell) increased for larger x and y lengths. The scenario remains the same with the increase of the number of atoms N to about ≈ 240000 , beyond which the number of droplets for large x and y lengths ($l_1 = l_2 \geq 18$) spontaneously increases from 25 (in the initial state) to 41 (in the final state) during imaginary-time propagation. If we compare plots (e) and (f), we find that with the increase in the size of the box trap from $l_1 = l_2 = 15$ to 18 for the fixed number $N = 300000$ of atoms, the number of droplets has spontaneously increased from 25 to 41 in the final state arranged in a square lattice inclined at an angle of 45° with respect to the initial square lattice. This 41-droplet state is composed of alternately placed five rows of five-droplet states and four rows of four-droplet states. The 41-droplet square-lattice state can be formed for $350000 > N > 240000$ and for large values of x and y lengths l_1, l_2 . For smaller values of l_1 and l_2 the number of droplets remain 25 in the final state and for large N ($N > 350000$), a larger number of droplets ($N > 41$) arranged on a distorted lattice without a periodicity can be formed (result not presented here). In plots (a)-(e) the unit cell of the lattice arrangement is the square lattice of Fig. 1(a) and the same in plot (f) is the centered square lattice of Fig. 1(b). All the states displayed in Fig. 2 have a maximum density at the center $x = y = 0$ and are parity-symmetric in x and y .

After having established the formation of a 25-droplet 5×5 square-lattice state in a dipolar BEC of ^{164}Dy atoms, we study the formation of 9-, 16-, 36-, 49-, 64-, and 81-droplet 3×3 , 4×4 , 6×6 , 7×7 , 8×8 , and 9×9 square-lattice states in a square box trap U_A and the results are displayed, respectively, in Fig. 3 for (a) $N = 45000$, x and y lengths $l_1 = l_2 = 5$, (b) $N = 80000$, $l_1 = l_2 = 10$, (c) $N = 180000$, $l_1 = l_2 = 15$, (d) $N = 245000$, $l_1 = l_2 = 15$, (e) $N = 512000$, $l_1 = l_2 = 16$, and (f) $N = 405000$, $l_1 = l_2 = 18$. In all cases the z -length of the box trap is $l_3 = 5$. These states were calculated in imaginary-time propagation using an analytic square-lattice initial state with the corresponding number of droplets appropriately arranged on a square lattice. For example, the initial function for a 81-droplet 9×9 square-lattice state is taken as in (9). In the case of an odd number of droplets, the size of the unit cell in (a), (d), and (f) are approximately equal, whereas the size of the unit cell in the case of an even number of droplets in (b), (c), and (e) are different and larger than the same in the case of an odd number of droplets.

The formation of a droplet lattice in a box trap is a bit different from that in a 3D harmonic potential as used in previous experimental [20–22, 25] and theoretical [33, 37–40] studies on the formation of a droplet lattice. In the case of a harmonically-trapped droplet-lattice state, the number

of atoms per droplet is approximately a constant depending on the parameters (scattering length and trap frequencies) of the problem; for ^{164}Dy atoms with $a = 85a_0$, this number is about 11000 atoms/droplet for the trap used in Ref. [26]. This number will be different for a different trap. But in the case of a square box trap the number of atoms per droplet can have a wide range of values. It is possible to have a 25-droplet square-lattice state in a square box trap with number of atoms/droplet varying from about 4000 to 9000, provided the x and y lengths are increased appropriately as the number of atoms is increased. If the x and y lengths are not increased, more droplets may appear in place of 25 droplets and the clean square-lattice structure is destroyed. In Fig. 3 we have chosen to show the results for 5000 atoms per droplet in all plots except in Fig. 3(e) with 8000 atoms per droplet. The possibility of the formation of a droplet lattice state for a small number of atoms in a box trap, as compared to the same in a harmonic trap, could facilitate the use of a box trap in experiments and also in theoretical investigations, as for a small number of atoms the nonlinearity of the model will be small.

The formation of a supersolid-like state in a square box trap is quite different from that in a harmonic trap; the former gives the unique opportunity to study a spatially-periodic state without the interference of an external trap. This crystallization of matter in free space bounded by a rigid wall, as encountered in a box trap, was the original conceptualization of a supersolid [1–4]. This has the advantage that by enlarging the boundary of the square box trap it is possible to increase the size of the square-lattice state as large as we wish without compromising the quality of the lattice and without the formation of an excessive atom cloud as in a harmonic potential trap [26]. This is illustrated in Fig. 4 for a square box trap U_A for (a) a 169-droplet 13×13 square-lattice state with $N = 840000$ atoms and x and y lengths $l_1 = l_2 = 26$, (b) a 196-droplet 14×14 square-lattice state with $N = 1180000$ atoms and x and y lengths $l_1 = l_2 = 28$, and (c) a 145-droplet state with $N = 1000000$ atoms and x and y lengths $l_1 = l_2 = 28$. In plot (a) [plot(b)], the central site at $x = y = 0$ is occupied (unoccupied) and it is a parity-symmetric (parity-antisymmetric) state in x and y . These states were obtained in imaginary-time simulation using analytic initial functions with the same number of droplets as in the final state placed appropriately, viz. Eq. (9). The unit cell in (a) and (b) is a square [as in Fig. 1(a)] and in (c) is a centered square [as in Figs. 1(b), and 2(f)]. In Fig. 4 (c), in-between nine rows of nine droplets each (present in the initial state), eight rows of eight droplets each are alternately created spontaneously during imaginary-time propagation so as to form a 145-droplet state. In all cases the droplet-lattice structure is very clean without an excessive atom cloud in the background and without any visible distortion. We verified that the reduced atom cloud, we have in

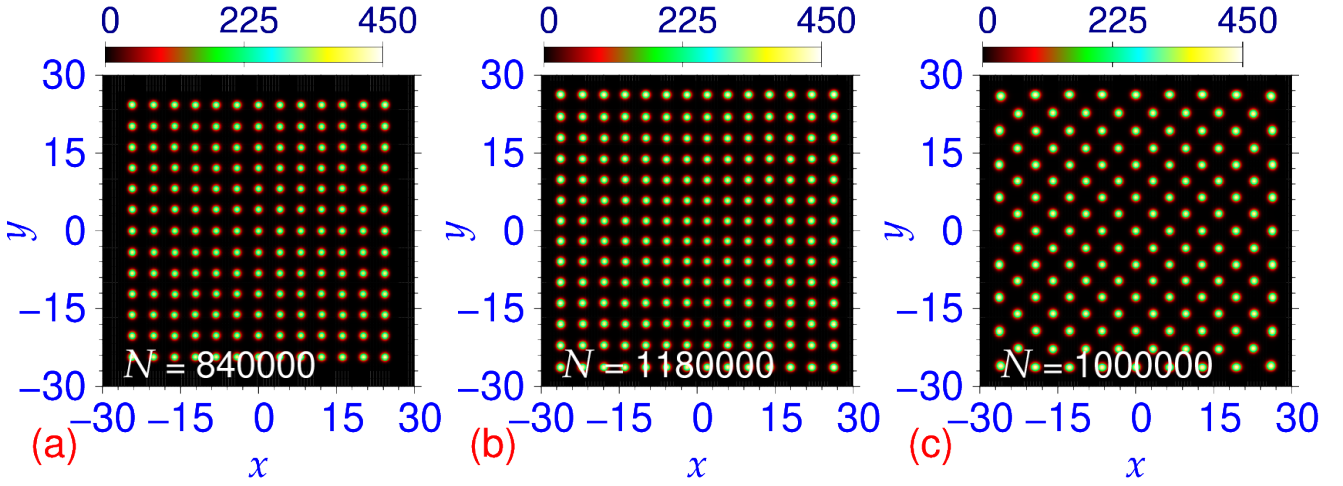


Fig. 4 Contour plot of density of ^{164}Dy atoms $N|\psi(x,y,0)|^2$ in the x - y plane of square-lattice crystallization in a (a) 169-droplet 13×13 square-lattice state with $N = 840000$ and x and y lengths $l_1 = l_2 = 26$, (b) 196-droplet 14×14 square-lattice state with $N = 1180000$ and $l_1 = l_2 = 28$, and (c) 145-droplet state with $N = 1000000$ and $l_1 = l_2 = 28$, in a 3D square box trap U_A . The unit cell in (a) and (b) is the square lattice of Fig. 1(a) and that in (c) is the centered square lattice of Fig. 1(b). The z -length in all cases is $l_3 = 5$ and $a = 85a_0$.

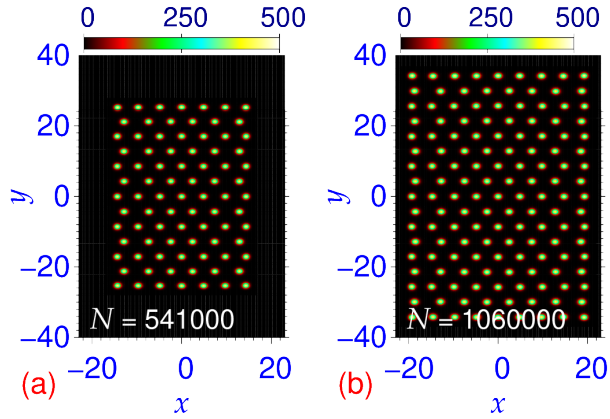


Fig. 5 Contour plot of density of ^{164}Dy atoms $N|\psi(x,y,0)|^2$ in the x - y plane of triangular-lattice crystallization of (a) 85 droplets with x length $l_1 = 16$ and y length $l_2 = 27$, (b) 145 droplets with x length $l_1 = 21$ and y length $l_2 = 36$, in a 3D rectangular box trap U_B . The z -length in all cases is $l_3 = 5$ and $a = 85a_0$.

a box potential, is of uniform density and which increases the background density by a small amount in all places and do not create any visible atom cloud in the background.

Some of these aspects have been studied in Ref. [53] for a slightly different box trap, e.g. a box trap in the x - y plane and a harmonic trap in the z direction, and for a slightly larger value of the scattering length of ^{164}Dy atoms, e.g. a in the range $90a_0$ to $100a_0$. Both these differences with Ref. [53] have possibly been fundamental in reducing the non-uniform background atom cloud and obtain very large droplet-lattice structure in this paper. Moreover, a spontaneous formation of square-lattice state making an angle of 45° with the boundary of the box potential, viz. Figs. 2(f) and 4(c), was not found before. Also, the possibility of the

formation of a lattice of different symmetry than that of the binding box potential, viz. Fig. 5, was not also explored previously.

It is intuitively expected that a periodic lattice state with a specific symmetry can efficiently be formed in a box trap with the same symmetry. A square box trap is suitable for the formation of a periodic square-lattice state. Similarly, a rectangular box trap (not considered here) is also suitable for the formation of a periodic square-lattice state. We will see in the following that a hexagonal box trap is suitable for the formation of a periodic triangular-lattice state. Nevertheless, a triangular-lattice state can also be realized in a rectangular box trap with appropriate sizes. The inclined square-lattice arrangements of Fig. 2(f) and 4(c) is made of small triangles with height-to-base ratio of $1 : 2$. If this ratio could be changed to $\sqrt{3} : 2$ by squeezing the lattice along x direction, the square-lattice arrangements of Fig. 4(c) will become a triangular-lattice arrangement. With this in mind we consider a rectangular box trap U_B with length to breadth ratio in the x - y plane $l_1 : l_2 \approx 1 : \sqrt{3}$. In such an appropriate trap the 85-droplet square-lattice state becomes a triangular-lattice state as shown in Fig. 5(a) through a contour plot of density of ^{164}Dy atoms $N|\psi(x,y,0)|^2$ in the x - y plane for $N = 541000$ atoms and x and y cut offs $l_1 = 16$ and $l_2 = 27$. In Fig. 5(b) we display contour plot of density of a 145-droplet triangular-lattice state for $N = 1060000$ atoms and x and y cut offs $l_1 = 21$ and $l_2 = 36$. The z -length in both cases is $l_3 = 5$. The initial state in imaginary-time simulation was one with the same number of droplets, and with the same symmetry, as the final state. In both these cases, unlike in Fig. 4(c), there is some distortion of the triangular lattice near the boundary, although there is no visible background cloud of atoms.

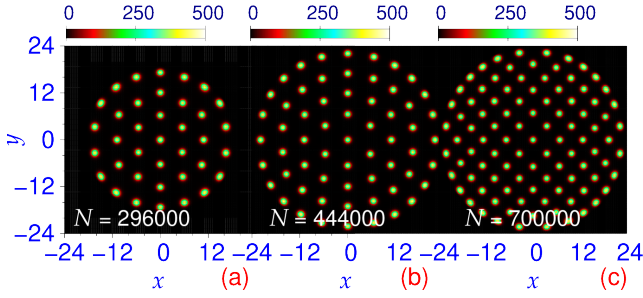


Fig. 6 Contour plot of density of ^{164}Dy atoms $N|\psi(x,y,0)|^2$ in the x - y plane of triangular-lattice crystallization of (a) 37 droplets with ρ length $l_1 = 19$, and (b) 61 droplets with ρ length $l_1 = 24$, and the same of square-lattice crystallization of (c) 97 droplets with ρ length $l_1 = 24$ in a 3D cylindrical box trap U_C . The z -length in all cases is $l_3 = 5$ and $a = 85a_0$.

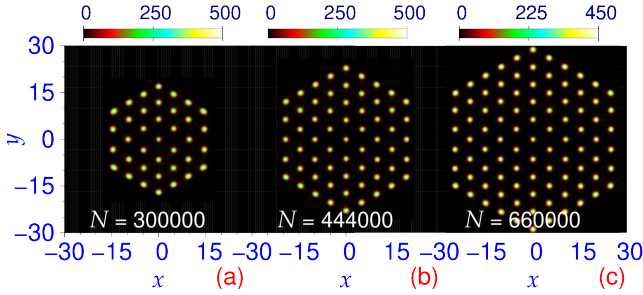


Fig. 7 Contour plot of density $N|\psi(x,y,0)|^2$ of triangular-lattice crystallization of ^{164}Dy atoms in a 3D hexagonal box trap U_D of (a) 37 droplets with length of each side of hexagon $l_1 = 19$, (b) 61 droplets with $l_1 = 25$, (c) 91 droplets with $l_1 = 31$. The z -length in all cases is $l_3 = 5$ and $a = 85a_0$.

We also studied the formation of a triangular- and a square-lattice arrangement of droplets in a cylindrical box potential by imaginary-time propagation using an initial state with the same symmetry and with an appropriate number of droplets. The contour plot of density of ^{164}Dy atoms $N|\psi(x,y,0)|^2$ in the x - y plane of 37- and 61-droplet triangular-lattice states for $N = 296000$ and $N = 444000$ so obtained are shown in Fig. 6(a)-(b), for $\rho \equiv \sqrt{x^2 + y^2}$ lengths (a) 19, (b) 24, respectively, with 3, and 4 concentric hexagonal orbits. The number of droplets in the concentric orbits of Fig. 6 are 6, 12, 18, 24, as in the concentric hexagons of a triangular-lattice structure. The contour plot of density of ^{164}Dy atoms $N|\psi(x,y,0)|^2$ in the x - y plane of a 97-droplet square-lattice state for $N = 700000$ is displayed in Fig. 6(c), for ρ length 24. The triangular- and square-lattice arrangements of the droplets can be clearly seen in Figs. 6(a)-(b), and (c), respectively, although there is some distortion of the lattice structure near the circular boundary.

The triangular-lattice state in a rectangular or a cylindrical box trap is usually distorted, specially in the outer orbits of the droplets. Next we demonstrate the formation of perfect triangular-lattice states in a hexagonal box trap U_D of

appropriate size, without any distortion. The initial function in imaginary-time simulation was taken to be a triangular-lattice state with the same number of droplets as in the final state. For example, the initial function for a 37-droplet triangular-lattice state is taken as in Eq. (10). The corresponding contour plot of densities in a hexagonal box trap U_D is illustrated in Fig. 7 for (a) 37 droplets with $N = 300000$ atoms and length of each side of hexagon $l_1 = 19$, (b) 61 droplets with $N = 444000$ atoms and $l_1 = 25$, and (c) 91 droplets with $N = 660000$ atoms and $l_1 = 31$. The distortion in the hexagonal lattice of Fig. 7 is practically invisible compared to that in Figs. 6(a)-(b) and also in Fig. 5, specially near the boundary of the box traps.

To demonstrate the dynamical stability of the droplet-lattice states we perform real-time simulation of the converged imaginary-time state during a long period of time. For this purpose we consider the newly-obtained droplet lattice states displayed in Figs. 2(c) and (f). The triangular-lattice state was already observed in different experiments [20, 25, 32], hence it is presumably dynamically stable. First we consider the square-lattice state of Fig. 2(c) obtained with a 3D square box trap with $l_1 = l_2 = 18, l_3 = 5$. A real-time calculation is performed with the converged imaginary-time state as the initial state after changing the size of the square box trap to $l_1 = l_2 = 18.25, l_3 = 5$. The square-lattice state expands a bit maintaining the structure of the initial 25-droplet 5×5 state and remains stable for a long time demonstrating its dynamical stability as illustrated through a contour plot of density $N|\psi(x,y,0)|^2$ in Fig. 8(a) at time $t = 40$. Now we consider the 41-droplet state of Fig. 2(f) obtained with a 3D square box trap with $l_1 = l_2 = 18, l_3 = 5$. To demonstrate its dynamical stability, a real-time calculation is performed with the converged imaginary-time state as the initial state after changing the size of the square box trap to $l_1 = l_2 = 18.25, l_3 = 5$. The state remains stable for a long time demonstrating its dynamical stability as illustrated through a contour plot of density $N|\psi(x,y,0)|^2$ in Fig. 8(b) at time $t = 40$.

4 Summary

Using a beyond-mean-field modified GP equation, we have demonstrated by imaginary-time propagation, including an LHY-type interaction [28, 29], supersolid-like spatially-periodic square-lattice and triangular-lattice crystallization of droplets of a quasi-2D dipolar BEC in square box (cuboid with two equal sides), rectangular box (cuboid), cylindrical box and hexagonal box (hexagonal prism) traps. The square box and hexagonal box traps are appropriate for the formation of spatially-periodic square-lattice and triangular-lattice states, respectively, and were used in the numerical investigation of these states. We find two types of square-lattice states in a square box trap, where the square-lattice structure could be

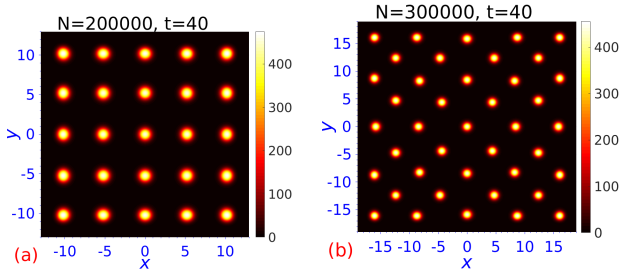


Fig. 8 (a) Contour plot of density of ^{164}Dy atoms $N|\psi(x,y,0)|^2$ in the x - y plane of the 25-droplet state of Fig. 2(e) in a 3D square box trap after real-time propagation for $t = 40$ time units after changing size of the square box trap from $l_1 = l_2 = 18, l_3 = 5$ to $l_1 = l_2 = 18.25, l_3 = 5$ at $t = 0$. (b) The same of the 25-droplet state of Fig. 2(f) in a 3D square box trap after real-time propagation for $t = 40$ time units after changing size of the square box trap from $l_1 = l_2 = 18, l_3 = 5$ to $l_1 = l_2 = 18.25, l_3 = 5$ at $t = 0$.

aligned parallel to the x and y axes or inclined at 45° with these axes. Nevertheless, we also studied the formation of triangular-lattice state in a rectangular box and circular box traps as well as the formation of a square-lattice state in a circular box trap. The triangular-lattice crystallization in a cylindrical or a rectangular box trap as well as the square-lattice crystallization in a cylindrical box trap are distorted near the boundary of the box trap. The dynamic stability of the droplet-lattice states was established by real-time propagation.

In a harmonically trapped dipolar BEC, it is difficult to form a very large droplet-lattice state without any deformation [26] whereas in a box trap a large droplet-lattice can be formed without a visible deformation and without a perceivable background cloud of atoms. Although, the first observation and study of a dipolar supersolid were made in a harmonically-trapped BEC, the presence of the interfering external trap possibly leads to a distorted lattice and will thus set a limitation on the formation of a large clean supersolid-like spatially-periodic lattice. A box trap, on the other hand, allows the formation of a spatially-ordered lattice of droplets in free space bounded by rigid walls, without any interfering potential, quite similar to an ideal supersolid conjectured in Refs. [1–4] in free space without any external potential. A droplet-lattice can be formed in a box potential for a significantly smaller number of atoms compared to the same in a harmonic potential [26], which could be an advantage in experimental realization of a large lattice of droplets in a box potential. At present moment, square, rectangular, and cylindrical box traps can be realized in a laboratory [44–51] and it is expected that a hexagonal box trap will follow soon. The results and conclusions of this paper can be tested in experiments with strongly dipolar quasi-2D atomic BECs of ^{164}Dy or ^{168}Er atoms with present knowhow.

Acknowledgments

SKA acknowledges support by the CNPq (Brazil) grant 301324/2019-0. LEY-S. would like to acknowledge the financial support by the Vicerrectoria de Investigaciones - Universidad de Cartagena through Project No. 019-2021.

Data Availability

Data Availability Statement: No Data associated in the manuscript

References

1. E. P. Gross, Phys. Rev. 106, 161 (1957)
2. A. F. Andreev and I. M. Lifshitz, Zurn. Eksp. Teor. Fiz. 56, 2057 (1969) [English Transla.: Sov. Phys. JETP 29, 1107 (1969)]
3. A. J. Leggett, Phys. Rev. Lett. 25, 1543 (1970)
4. G. V. Chester, Phys. Rev. A 2, 256 (1970)
5. M. Boninsegni and N. V. Prokofev, Rev. Mod. Phys. 84, 759 (2012)
6. V. I. Yukalov, Physics 2, 49 (2020)
7. D. Mihalache, Rom. Rep. Phys. 73, 403 (2021)
8. E. Kim and M. H. W. Chan, Nature (London) 427, 225 (2004)
9. S. Balibar, Nature (London) 464, 176 (2010)
10. Y. Li, G. I. Martone, L. P. Pitaevskii, S. Stringari, Phys. Rev. Lett. 110, 235302 (2013)
11. V. S. Bagnato, D. J. Frantzeskakis, P. G. Kevrekidis, B. A. Malomed, D. Mihalache, Rom. Rep. Phys. 67, 5 (2015)
12. Y. V. Kartashov, G. E. Astrakharchik, B. A. Malomed, L. Torner, Nature Reviews Physics 1, 185 (2019)
13. Z.-K. Lu, Y. Li, D. S. Petrov, G. V. Shlyapnikov, Phys. Rev. Lett. 115, 075303 (2015)
14. F. Wächtler, L. Santos, Phys. Rev. A 93, 061603(R) (2016)
15. F. Cinti, T. Macrì, W. Lechner, G. Pupillo, T. Pohl, Nat. Commun. 5, 3235 (2014)
16. J.-R. Li, J. Lee, W. Huang, S. Burchesky, B. Shteynas, F. Ç. Top, A. O. Jamison, W. Ketterle, Nature (London) 543, 91 (2017)
17. L. Tanzi, E. Lucioni, F. Famà, J. Catani, A. Fioretti, C. Gabbanini, R. N. Bisset, L. Santos, G. Modugno, Phys. Rev. Lett. 122, 130405 (2019)
18. F. Böttcher, J.-N. Schmidt, M. Wenzel, J. Hertkorn, M. Guo, T. Langen, T. Pfau, Phys. Rev. X 9, 011051 (2019)
19. L. Chomaz, D. Petter, P. Ilzhöfer, G. Natale, A. Trautmann, C. Politi, G. Durastante, R. M. W. van Bijnen, A. Patscheider, M. Sohmen, M. J. Mark, F. Ferlaino, Phys. Rev. X 9, 021012 (2019)

20. M. Schmitt, M. Wenzel, F. Böttcher, I. Ferrier-Barbut, and T. Pfau, *Nature (London)* 539, 259 (2016)
21. L. Chomaz, S. Baier, D. Petter, M. J. Mark, F. Wächtler, L. Santos, F. Ferlaino, *Phys. Rev. X* 6, 041039 (2016)
22. H. Kadau, M. Schmitt, M. Wenzel, C. Wink, T. Maier, I. Ferrier-Barbut, T. Pfau, *Nature (London)* 530, 194 (2016)
23. I. Ferrier-Barbut, H. Kadau, M. Schmitt, M. Wenzel, T. Pfau, *Phys. Rev. Lett.* 116, 215301 (2016)
24. G. Natale, R. M. W. van Bijnen, A. Patscheider, D. Petter, M. J. Mark, L. Chomaz, F. Ferlaino, *Phys. Rev. Lett.* 123, 050402 (2019)
25. M. A. Norcia, C. Politi, L. Klaus, E. Poli, M. Sohmen, M. J. Mark, R. Bisset, L. Santos, F. Ferlaino, *Nature (London)* 596, 357 (2021)
26. L. E. Young-S., S. K. Adhikari, *Phys. Rev. A* 105, 033311 (2022)
27. T. D. Lee, K. Huang, C. N. Yang, *Phys. Rev.* 106, 1135 (1957)
28. A. R. P. Lima, A. Pelster, *Phys. Rev. A* 84, 041604(R) (2011)
29. A. R. P. Lima, A. Pelster, *Phys. Rev. A* 86, 063609 (2012)
30. F. Wächtler, L. Santos, *Phys. Rev. A* 94, 043618 (2016)
31. R. N. Bisset, R. M. Wilson, D. Baillie, P. B. Blakie, *Phys. Rev. A* 94, 033619 (2016)
32. T. Bland, E. Poli, C. Politi, L. Klaus, M. A. Norcia, F. Ferlaino, L. Santos, R. N. Bisset, *Phys. Rev. Lett.* 128, 195302 (2022)
33. E. Poli, T. Bland, C. Politi, L. Klaus, M. A. Norcia, F. Ferlaino, R. N. Bisset, L. Santos, *Phys. Rev. A* 104, 063307 (2021)
34. M. Guo, F. Böttcher, J. Hertkorn, J.-N. Schmidt, M. Wenzel, H. P. Büchler, T. Langen, T. Pfau, *Nature (London)* 574, 386 (2019)
35. L. Tanzi, S. Roccuzzo, E. Lucioni, F. Famà, A. Fioretti, C. Gabbanini, G. Modugno, A. Recati, S. Stringari, *Nature (London)* 574, 382 (2019)
36. R. Bombin, J. Boronat, F. Mazzanti, *Phys. Rev. Lett.* 119, 250402 (2017)
37. D. Baillie, P. B. Blakie, *Phys. Rev. Lett.* 121, 195301 (2018)
38. Y.-C. Zhang, T. Pohl, F. Maucher, *Phys. Rev. A* 104, 013310 (2021)
39. J. Hertkorn, J.-N. Schmidt, M. Guo, F. Böttcher, K. S. H. Ng, S.D. Graham, P. Uerlings, T. Langen, M. Zwierlein, T. Pfau, *Phys. Rev. Research* 3, 033125 (2021)
40. Y.-C. Zhang, F. Maucher, T. Pohl, *Phys. Rev. Lett.* 123, 015301 (2019)
41. J. Léonard, A. Morales, P. Zupancic, T. Esslinger, T. Donner, *Nature (London)* 543, 87 (2017)
42. P. Kaur, S. Gautam, S. K. Adhikari, *Phys. Rev. A* 105, 023303 (2022)
43. S. K. Adhikari, *J. Phys.: Condens. Matter* 33, 265402 (2021)
44. T. P. Meyrath, F. Schreck, J. L. Hanssen, C.-S. Chuu, M. G. Raizen, *Phys. Rev. A* 71, 041604(R) (2005)
45. S. Gupta, K. W. Murch, K. L. Moore, T. P. Purdy, and D. M. Stamper-Kurn, *Phys. Rev. Lett.* 95, 143201 (2005)
46. J. J. P. van Es, P. Wicke, A. H. van Amerongen, C. Rétif, S. Whitlock, N. J. van Druten, *J. Phys. B: At. Mol. Opt. Phys.* 43, 155002 (2010)
47. T. F. Schmidutz, I. Gotlibovych, A. L. Gaunt, R. P. Smith, N. Navon, Z. Hadzibabic, *Phys. Rev. Lett.* 112, 040403 (2014)
48. A. L. Gaunt, T. F. Schmidutz, I. Gotlibovych, R. P. Smith, Z. Hadzibabic, *Phys. Rev. Lett.* 110, 200406 (2013)
49. N. Navon, A. L. Gaunt, R. P. Smith, Z. Hadzibabic, *Nature (London)* 539, 72 (2016)
50. S. J. Garratt, C. Eigen, J. Zhang, P. Turzák, R. Lopes, R. P. Smith, Z. Hadzibabic, N. Navon, *Phys. Rev. A* 99, 021601(R) (2019)
51. R. Lopes, C. Eigen, N. Navon, D. Clément, R. P. Smith, Z. Hadzibabic, *Phys. Rev. Lett.* 119, 190404 (2017)
52. E. Busley, L. E. Miranda, A. Redmann, C. Kurtscheid, K. K. Umesh, F. Vewinger, M. Weitz, J. Schmitt, *Science* 375, 1403 (2022)
53. S. M. Roccuzzo, S. Stringari, A. Recati, *Phys. Rev. Research* 4, 013086 (2021)
54. B. Kh. Turmanov, B. B. Baizakov, F. Kh. Abdullaev, M. Salerno, *J. Phys. B: At. Mol. Opt. Phys* (2021)
55. S. Datta, U. R. Fischer, *Phys. Rev. D* 105, 022003 (2022)
56. A. Romero-Ros, G. C. Katsimiga, P. G. Kevrekidis, B. Prinari, G. Biondini, P. Schmelcher, *Phys. Rev. A* 103, 023329 (2021)
57. T. Lahaye, C. Menotti, L. Santos, M. Lewenstein, T. Pfau, *Rep. Prog. Phys.* 72, 126401 (2009)
58. R. Kishor Kumar, L. E. Young-S., D. Vudragović, A. Balaž, P. Muruganandam, S. K. Adhikari, *Comput. Phys. Commun.* 195, 117 (2015)
59. V. I. Yukalov, *Laser Phys.* 28, 053001 (2018)
60. L. Chomaz, I. Ferrier-Barbut, F. Ferlaino, B. Laburthe-Tolra, B. L. Lev, T. Pfau, *arXiv:2201.02672*.
61. P. Muruganandam, S. K. Adhikari, *Comput. Phys. Commun.* 180, 1888 (2009)
62. V. Lončar, L. E. Young-S., S. Škrbić, P. Muruganandam, S. K. Adhikari, A. Balaž, *Comput. Phys. Commun.* 209, 190 (2016)
63. D. Vudragović, I. Vidanović, A. Balaž, P. Muruganandam, S. K. Adhikari, *Comput. Phys. Commun.* 183, 2021 (2012)
64. Y. Tang, A. Sykes, N. Q. Burdick, J. L. Bohn, B. L. Lev, *Phys. Rev. A* 92, 022703 (2015)